

Identification of variation coefficient of equivalent stress range of steel girders with cracks

Z. Kala, A. Omishore, S. Seitl, M. Krejsa, J. Kala

Abstract —A steel bridge in operation is subjected to multiple variable stress range spectrum from the passage of axles of vehicles of different weights. The fatigue reliability assessment of steel bridges can be performed using the equivalent stress range, which is converted from the variable stress range spectrum. The paper presents a case study of the identification of the coefficient of variation of the equivalent stress range of steel girders. The histogram of equivalent stress range is statistically evaluated with consideration to uncertainties resulting from the statistical evaluation of the histogram of stress range spectrum from field monitoring. It is shown that the equivalent stress range can be rationally considered as a random variable with Gauss probability density function with coefficient of variation of 0.1. The case study is evaluated using the Latin Hypercube Sampling statistical method. The results are exploitable in the probabilistic analyses of reliability and lifetime of bridges using linear elastic fracture mechanics.

Keywords — Equivalent stress range, fatigue, bridge, steel, linear fracture mechanics, probability, reliability.

I. INTRODUCTION

Structural fatigue occurs whenever a bridge structure is subjected to time varying loads [1, 2]. Each time a load cycle is applied, an incremental amount of damage occurs. This damage is cumulative in nature and accumulation continues until failure occurs.

Recently, a number of different methods have been proposed for estimating the fatigue life of steel bridges. For instance, Righiniotis [3] concluded that the fatigue life of steel

railway bridges subjected to increasing rail traffic load is drastically reduced when the rail traffic load is increased to a certain degree. Rao and S. Talukdar proposed a systematic approach based on the linear damage theory to calculate the fatigue life of a bridge with respect to its dynamic interaction with a vehicle [4]. Leander and Al-Emrani [5] identified the significant influence of material parameters and stress intensity factor on the reliability index β using linear elastic fracture mechanics and sensitivity analysis. Leander [6] proposed a probabilistic model for fatigue life prediction based on vehicle data from bridge weigh-in-motion measurements. Kim et al. [7] developed a fatigue prediction model based on using the measured variable stress spectra of three steel bridges. Nagy et al. [8] experimentally investigated crack propagation in orthotropic steel decks near the weld connecting the longitudinal stiffener. Hasni et al. [9] introduced the use of artificial intelligence in processing strain data from wireless sensors mounted on steel bridge girders.

The effective prediction of the fatigue life of steel bridge members susceptible to fatigue requires timely decision making for maintenance and rehabilitation planning [10, 11]. The current trend in these works is not the use of one, but of multiple MCDM methods in problems of ranking and selection [12-14].

The basis for predicting the fatigue life in the complicated time history is empirical data from laboratory tests with constant amplitude [15-17]. Laboratory tests confirm that fatigue failure depends significantly only on the minimum and maximum values of stresses during the cycle. Practically, the random fatigue loading process can be replaced by a periodic load process that is defined as a constant amplitude load cycle.

The equivalent stress range is defined on the basis of the minimum and maximum values of stresses during the cycles, which cause the same fatigue damage as from the complicated random traffic load. It is shown in paper [18] that the equivalent stress range is a random variable with random variability due to uncertainties associated with the load history, which can be expressed using several probability density functions (Lognormal, Weibull or Gamma).

The aim of this paper is to determine the value of the coefficient of variation of the equivalent stress range, which is associated with uncertainties associated with the load history.

It is shown in the article that the introduction of the

This result was achieved with the financial support of the projects 17-01589S and No. LO1408 "AdMAs UP".

Zdeněk Kala is with the Brno University of Technology, Faculty of Civil Engineering, Brno, ZIP 602 00 CZ (phone: +420-541147382; fax: +420-541240994; e-mail: kala.z@fce.vutbr.cz).

Abayomi Omishore is with the Brno University of Technology, Faculty of Civil Engineering, Brno, ZIP 602 00 CZ (phone: +420-541147369; fax: +420-541240994; e-mail: omishore.a@fce.vutbr.cz).

Stanislav Seitl is with the Institute of Physics of Materials of the Academy of Sciences of the Czech Republic, Brno, ZIP 616 62 CZ (phone: +420-532290361; fax: +420-541218657; e-mail: seitl@ipm.cz).

Martin Krejsa is with the VŠB - Technical University of Ostrava, Faculty of Civil Engineering, Ostrava, ZIP 708 33 CZ (phone: +420-597321303; fax: +420-597321318; e-mail: martin.krejsa@vsb.cz).

Jiří Kala is with the Brno University of Technology, Faculty of Civil Engineering, Brno, ZIP 602 00 CZ (phone: +420-541147392; fax: +420-541240994; e-mail: kala.j@fce.vutbr.cz).

equivalent stress range as a random variable is justified. The basic types of probability density functions for the appropriate modelling of the equivalent stress range are presented.

II. FATIGUE LIFE ASSESSMENT OF STEEL BRIDGES

Many old bridges cannot be renovated or replaced within a reasonable budget constraint. However, their lifetime should be extended as much as possible for reasons of sustainability [19]. The estimation of the residual life requires the use of sophisticated reliability assessment methods. A gradual increase in the complexity and sophistication of various levels of evaluation, from common standard-based methods to advanced methods based on fracture mechanics and probability assessment, can be expected. On the other hand, computational models that describe more complex phenomena will typically require more input variables and modelling options that are affected by uncertainty. This leads to a greater need for reliable information regarding the properties and actual state of the structure.

A. Linear Elastic Fracture Mechanics

Linear elastic fracture mechanics is based on the analysis of cracks in linear elastic materials. It can be used to solve most practical problems in mechanical and civil engineering, such as the estimation of reliability and lifetime of load bearing steel structures with cracks. The theory is based on linearity making it possible to easily combine theoretical, numerical and experimental analyses of fracture.

Fatigue crack growth is generally described by Paris's rule, which is expressed by Paris and Erdogan [20].

$$\frac{da}{dN} = C \cdot (\Delta K)^m \quad (1)$$

Equation (1) describes the behaviour of cracked materials subjected to many times repeated loading and implies the knowledge of both the stress intensity factor (ΔK) and the crack growth rate (da/dN), where m and C are material-related parameters. The parameter C can be expressed as

$$\log(C) = c_1 + m \cdot c_2, \quad (2)$$

where c_1 , c_2 can be considered for steel grade S235 as $c_1 = -11.141$, $c_2 = -0.507$ [21]. The range of stress intensity factor ΔK can be determined by Broek [22].

$$\Delta K = \Delta \sigma \cdot \sqrt{\pi a} \cdot f(a), \quad (3)$$

where $\Delta \sigma$ is the quasi-constant stress range and $f(a)$ is the calibration function (geometric factor) obtained from experimental and numerical research, see for e.g. [15-17]. The calibration function $f(a)$ is member-specific and may not be applicable for other cases. However, many types of calibration functions can be found in handbooks [23, 24].

By substituting Eq. (3) into Eq. (1) and then integrating it, we can obtain a relationship that determines crack propagation from length a_1 to a_2 due to the effects of the number of cycles from N_1 to N_2 .

$$\int_{a_1}^{a_2} \frac{da}{[f(a) \cdot \sqrt{\pi \cdot a}]^m} = \int_{N_1}^{N_2} C \cdot \Delta \sigma^m dN. \quad (4)$$

In bridge structures, a crack may propagate from the initial size a_0 to the critical size a_{cr} right from the first load cycle from the passage of the first vehicle. Fatigue crack initiation often occurs at an inclusion, impurity or surface flaw, which acts as a local stress raiser and results in small scale plastic deformation. Under this assumption, we can substitute $a_1 = a_0$, $a_2 = a_{cr}$, $N_1 = 0$ and $N_2 = N$ in Eq. 4, where N is the total number of cycles that cause crack propagation from length a_1 to a_2 .

$$\int_{a_0}^{a_{cr}} \frac{da}{[f(a) \cdot \sqrt{\pi \cdot a}]^m} = C \cdot N \cdot \Delta \sigma^m. \quad (5)$$

The quasi-constant stress range $\Delta \sigma$ of longitudinal stress is written on the right side of Eq. (5). A real bridge is subjected to varying stress range spectrum from the passage of axles of vehicles of different weights. For the purpose of taking the stress range spectrum from the histogram, the right side of equation (5) can be substituted by the sum:

$$C \cdot N \cdot \Delta \sigma^m \approx C \cdot \sum_{i=1}^M (n_i \cdot \Delta \sigma_i^m), \quad (6)$$

where $\Delta \sigma_j$ are direct stress ranges representing class intervals of the spectrum, n_i is the frequency of amplitudes in these spectrums and M is the total number of classes of the spectrum. It can be written that the sum of all n_i is equal to N .

$$\sum_{i=1}^M n_i = N. \quad (7)$$

In the limit case, one stress range and one frequency fall into each class. On this basis, Eq. (7) can be modified as:

$$C \cdot \sum_{i=1}^M (n_i \cdot \Delta \sigma_i^m) \approx C \sum_{j=1}^N \Delta \sigma_j^m, \quad (8)$$

where $\Delta \sigma_j$ are direct stress ranges. Substituting (8) into (6) and subsequently into (5) we can write

$$\int_{a_0}^{a_{cr}} \frac{da}{[f(a) \cdot \sqrt{\pi \cdot a}]^m} = C \sum_{j=1}^N \Delta \sigma_j^m. \quad (9)$$

B. Equivalent Stress Range

By comparing (9) and (5) or (8) and (6) the histogram of direct stress range spectrum can be replaced by the equivalent stress range $\Delta \sigma_E$, which can be determined from Eq. (10):

$$\Delta\sigma_E = \left(\frac{1}{N} \sum_{j=1}^N \Delta\sigma_j^m \right)^{\frac{1}{m}}. \quad (10)$$

For N cycles, the equivalent stress range $\Delta\sigma_E$ should cause the same fatigue damage as the direct stress range spectrum expressed by the histogram. Therefore, it is necessary in the sum in Eq. (10) to omit small values $\Delta\sigma_j < \Delta\sigma_L$, which do not cause fatigue damage, where $\Delta\sigma_L$ is the cut-off limit [18].

The cut-off limit $\Delta\sigma_L$ is the limit below which stress ranges of the design spectrum do not contribute to the calculated cumulative damage [6]. Standard [25] determines $\Delta\sigma_L$ using S-N curves. Standard [25] determines the cut-off limit $\Delta\sigma_L$ for direct stress ranges at the number of cycle $N_L=1E8$. The application of S-N curves [26] is well established in structural design [27], however, information pertaining to time-variable load and the detection of cracks from measurement carried out during the operational period of a bridge cannot be incorporated into reliability calculations [28]. The basic tools for these calculations are provided by fracture mechanics. According to Eq. (5) $\Delta\sigma_L$ can theoretically be written as

$$\Delta\sigma_L = \sqrt[m]{\frac{1}{C \cdot N_L} \int_{a_0}^{a_{cr}} \frac{da}{[f(a) \cdot \sqrt{\pi \cdot a}]^m}}. \quad (11)$$

Eq (11) provides an approximate calculation of $\Delta\sigma_L$. However, it is necessary to know the size of a_0 and other material parameters that are generally random and thus point to the random nature of $\Delta\sigma_L$. The uncertainty of $\Delta\sigma_L$ is one of the causes of the uncertainty of $\Delta\sigma_E$.

Other sources of the uncertainty of the equivalent stress range $\Delta\sigma_E$ are the conditions of investigation and evaluation of the measurements of $\Delta\sigma_j$ [18]. Direct stress range histograms are produced by using the rain-flow cycle counting method [18]. This method is generally accepted and is used for the assessment of fatigue.

Generally, there exist two types of tests to investigate live load effects: controlled and uncontrolled tests [18]. Controlled live load tests are used to investigate the effects of vehicle speed and position on the bridge deck, whilst uncontrolled live loading tests are used to investigate the overall influence of real traffic. Stress range histogram data are usually collected during the uncontrolled monitoring. The equivalent stress range and average daily traffic are calculated on the basis of the stress-range histogram created from the long-term monitoring program. As a result of loading uncertainties, a probabilistic approach, which considers various probability density functions for the load effects, can be used for predicting stress ranges during the fatigue lifetime.

III. COMPUTATION OF PROBABILITY DENSITY FUNCTIONS OF EQUIVALENT STRESS RANGE - CASE STUDY

Identification of the random variability of the equivalent stress range $\Delta\sigma_E$ can be performed using the methodological

procedure that is presented in the following case study. Let us consider a histogram of direct stress range spectrum, which was obtained from monitoring on a real bridge, see Fig. 1. The statistical characteristics of the histogram in Fig. 1 are listed in Table 1. The histogram data is uncertain for the reasons described in [18].

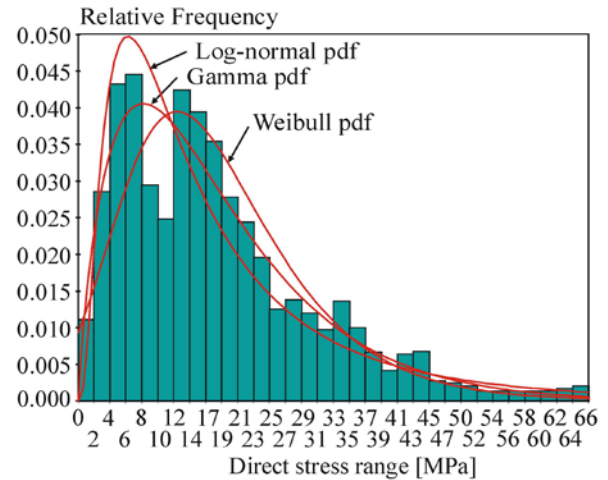


Fig. 1 Histogram of stress range spectrum based on measurements

In article [18] it is recommended to approximate the histogram using Gamma, Weibull or log-normal probability density functions (pdfs) after the application of the goodness of fit tests.

TABLE I
STATISTICAL CHARACTERISTICS OF HISTOGRAM IN FIG. 1

Characteristic	Value
Valid observations	100000
Minimum	0.00045
Maximum	65.998
Range	65.997
Median	15.355
Arithmetic mean	18.000
Geometric mean	13.490
Mean square	161.51
Variance	161.51
Stand. deviation	12.709
Coef. of variation	0.70615
Third moment	2402.4
Stand. skewness	1.1705
Fourth moment	0.11214E+06
Stand. kurtosis	4.2992
Variance of mean	0.0016151
Var. of variance	0.12539E+06
Var. of 3. moment	766.95
Var. of 4. moment	0.19628E+07

Kolmogorov-Smirnov goodness of fit test does not reject the hypothesis that the histogram has a Weibull or log-normal probability density function. Anderson-Darling goodness of fit test does not reject the hypothesis that the histogram has a Gamma, Weibull or log-normal probability density function.

Let the shape of the histogram have one of these three probability density functions. The values of the direct stress

range are positive (lower limit) and are limited by an upper limit beyond which excessive static loading or failure of the bridge may occur. This upper limit may be related, for example, to the maximum weight of the vehicle that may pass over the bridge.

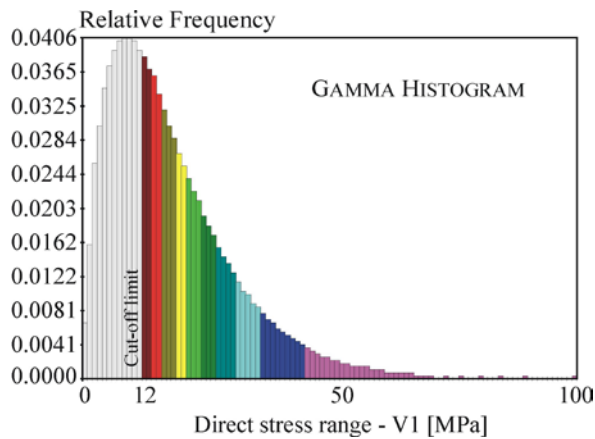


Fig. 2 Histogram acc. to Gamma probability density function

Histograms for the case study in Fig. 2 to Fig. 4 are defined in the interval [0, 100 MPa] and fit the shapes of Gamma, Weibull or log-normal probability density functions from Fig. 1. The nonparametric histograms in Fig. 2 to Fig. 4 effectively replace the parametric probability density functions from Fig. 1.

TABLE II

STATISTICAL CHARACTERISTICS OF HISTOGRAM IN FIG. 2

Characteristic	Value
Valid observations:	100000
Minimum:	0.1681
Maximum:	99.765
Range:	99.597
Median:	15.058
Arithmetic mean:	18.000
Geometric mean:	13.726
Mean square:	161.52
Variance:	161.52
Stand. deviation:	12.709
Coef. of variation:	0.70606
Third moment:	2805.1
Stand. skewness:	1.3665
Fourth moment:	0.14671E+06
Stand. kurtosis:	5.6236
Variance of mean	0.0016152
Var. of variance:	0.21475E+06
Var. of 3. moment:	2596.3
Var. of 4. moment:	0.13616E+08

The statistical characteristics of the histogram in Fig. 2 are listed in Table 2. It is evident that the histogram in Fig. 2 based on Gamma probability density functions has the same mean value and standard deviation as the histogram in Fig. 1 (see Table 1), but values of standard skewness and kurtosis are different.

The histogram in Fig. 3 is created after the negative values

of Weibull probability density functions have been cut-off and therefore the first three statistical moments are slightly different, nevertheless the standard kurtosis value of 4.13 is relatively close to the histogram in Fig. 1 (compared to 5.62 from Table II).

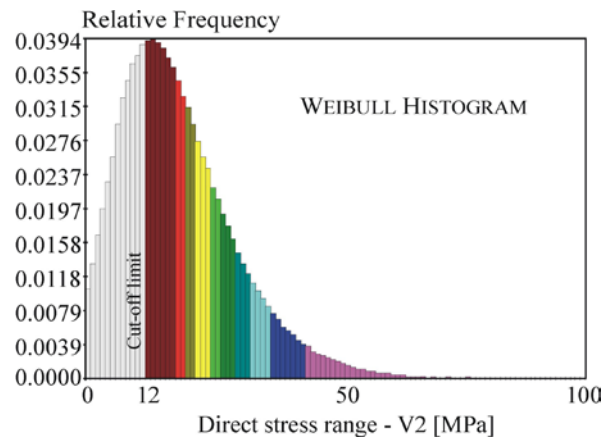


Fig. 3 Histogram acc. to Weibull probability density function

The histogram in Fig. 3 assumes a slightly higher frequency of occurrence of vehicles with almost zero weight and has a lower frequency of occurrence of very heavy vehicles (compared to Fig. 2).

TABLE III

STATISTICAL CHARACTERISTICS OF HISTOGRAM IN FIG. 3

Characteristic	Value
Valid observations:	100000
Minimum	0.00048
Maximum	76.977
Range	76.977
Median:	16.702
Arithmetic mean	18.596
Geometric mean	14.680
Mean square:	129.58
Variance	129.58
Stand. deviation	11.384
Coef. of variation:	0.61214
Third moment	1425.2
Stand. skewness	0.96615
Fourth moment:	69367.
Stand. kurtosis	4.1310
Variance of mean:	0.0012958
Var. of variance:	47938.0
Var. of 3. moment:	464.69
Var. of 4. moment:	0.12348E+07

The histogram in Fig. 4 is based on the log-normal probability density function in Fig. 1. The truncated log-normal histogram is found in the interval [0, 100] MPa and thus the mean value and standard deviation are the same as for the histogram in Fig. 1. (see Table 1), but the values of standard skewness and kurtosis are different. In particular, the high standard kurtosis value of 15.018 (see Table IV) differs greatly from the value of 4.2992 in Table 1.

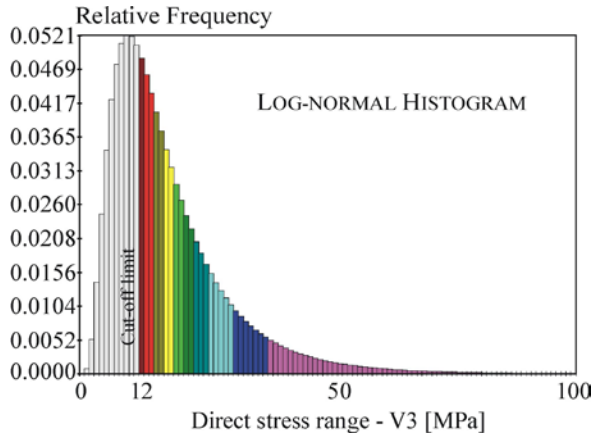


Fig. 4 Histogram acc. to log-normal probability density function

The histogram in Fig. 4 assumes zero frequency of occurrence of vehicles with zero weight.

TABLE IV

STATISTICAL CHARACTERISTICS OF HISTOGRAM IN FIG. 4

Characteristic	Value
Valid observations:	100000
Minimum:	0.8859
Maximum:	244.05
Range:	243.17
Median:	14.704
Arithmetic mean:	18.000
Geometric mean:	14.704
Mean square:	161.44
Variance:	161.44
Stand. deviation:	12.706
Coef. of variation:	0.70590
Third moment:	5037.6
Stand. skewness:	2.4558
Fourth moment:	0.39142E+06
Stand. kurtosis:	15.018
Variance of mean:	0.0016144
Var. of variance:	0.15308E+07
Var. of 3. moment:	46465.0
Var. of 4. moment:	0.13532E+10

The mean value of $\Delta\sigma_L$ is considered as 12 MPa in all cases. The randomness of $\Delta\sigma_L$, which is one of the causes of the randomness of the equivalent stress range $\Delta\sigma_E$, was taken into account with regard to the application of Eq. (10).

When calculating the equivalent stress range $\Delta\sigma_E$, equation (10) is modified to include only $\Delta\sigma_j > \Delta\sigma_L$, which are responsible for fatigue damage, see Eq. (12).

$$\Delta\sigma_E = \left(\frac{1}{N_C} \sum_{j=1}^{N_C} \Delta\sigma_j^m \right)^{\frac{1}{m}} \quad (12)$$

Equation (12) considers only N_C values of $\Delta\sigma_j | \Delta\sigma_j > \Delta\sigma_L$, where $N_C \leq N$, for the calculation of the equivalent stress range $\Delta\sigma_E$. Conversely, $\Delta\sigma_j \leq \Delta\sigma_L$ do not cause fatigue damage and are not considered in Eq. (12). In the present study, two alternatives A1 and A2 of the randomness of the cut-off limit

are considered, see Fig. 5 and Fig. 6. Alternative A1 assumes Gauss probability density function of cut-off limit with cut-off negative values, see Fig. 5 Alternative A2 assumes log-normal probability density function for cut-off limit, see Fig. 6.

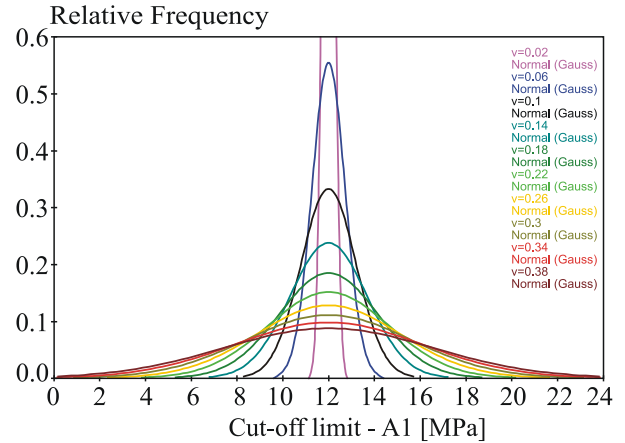


Fig. 5 Selected variants of cut-off limit with Gauss pdf

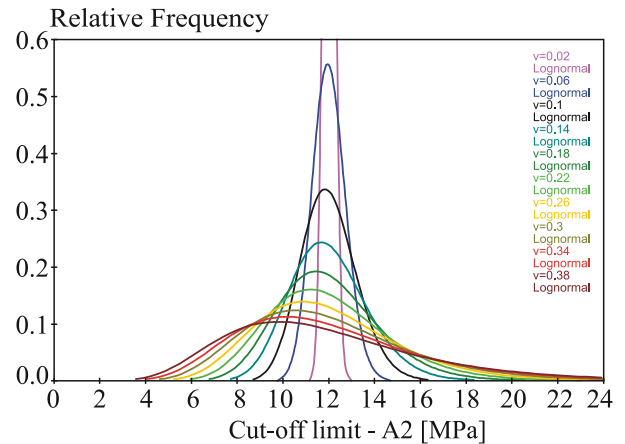


Fig. 6 Selected variants of cut-off limit with log-normal pdf

The equivalent stress range $\Delta\sigma_E$ is evaluated according to Eq. (12) using the Latin Hypercube Sampling (LHS) method [29, 30]. The flowchart of the computation of $\Delta\sigma_E$ is shown in Fig. 7. Practically, we can proceed as follows:

The coefficient of variation of the cut-off limit is chosen, for example $v=0.2$, alternative A1, see Fig. 5. 100 random samplings of the cut-off limit are simulated using the LHS method for this coefficient of variation. The first random realization of the equivalent stress range $\Delta\sigma_E$ is evaluated using 100 thousand random samplings simulated using the Gamma histogram in Fig. 2 so that the random realizations smaller than the cut-off limit are not applied in the sum (12). This procedure is repeated 100 times for other random realizations of the cut-off limit. Each random realization of the cut-off limit leads to one random realization of $\Delta\sigma_E$, which is evaluated using 100 thousand random sampling simulated from the Gamma histogram in Fig. 2. Another 100 random realizations of $\Delta\sigma_E$ are obtained in a similar manner for the histograms in Fig. 3 and Fig. 4. In total, three times a hundred random realizations of $\Delta\sigma_E$ are obtained, from which the histogram of $\Delta\sigma_E$ is then plotted, see Fig. 8.

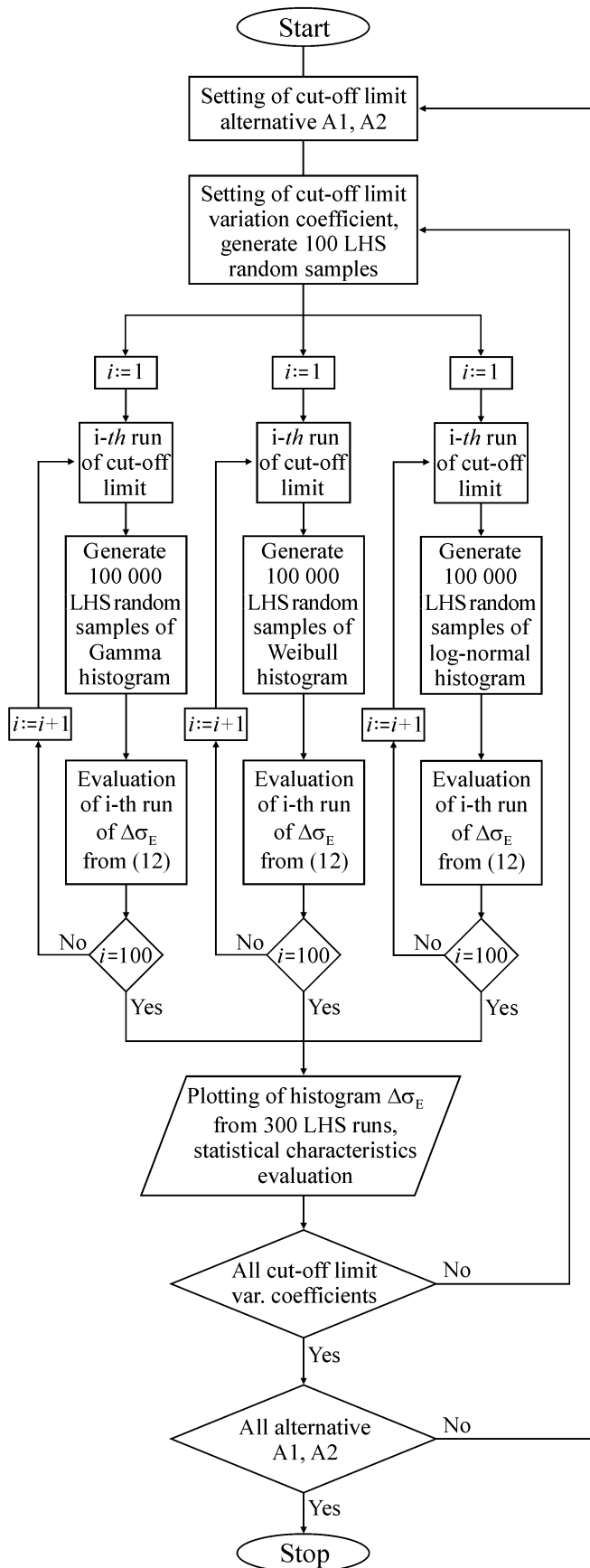


Fig. 7 Flow chart of the computation of $\Delta\sigma_E$

A detailed statistical evaluation of the histogram in Fig. 8 is in Table V. The mean value, standard deviation and coefficient of variation of the histogram in Fig. 8 are plotted as points (outputs) in the graphs and the procedure is repeated for other input values of the cut-off limit variant.

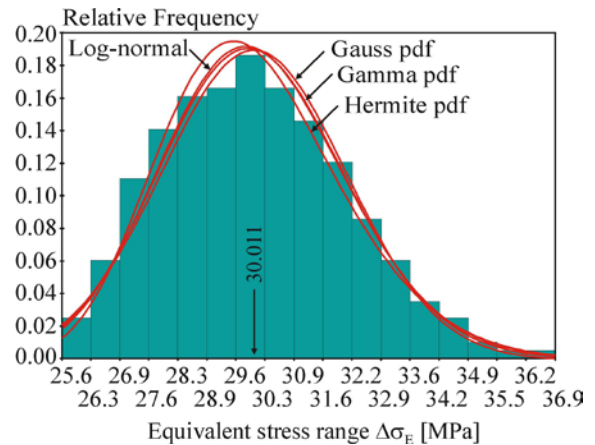


Fig. 8 Histogram for cut-off limit A1, $\nu=0.2$.

The histogram shown in Fig. 8 is evaluated from three hundred random realizations of $\Delta\sigma_E$, where each is calculated by applying Eq. (12) using the Gamma histogram, Weibull histogram and log-normal histogram and using the random realizations of the cut-off limit based on the Gauss probability density function with $\nu=0.2$. The histogram in Fig. 8 takes into account the overall uncertainty of the approximation of the original histogram in Fig. 1. A detailed statistical evaluation of the histogram in Fig. 8 is presented in Table V.

TABLE V
STATISTICAL CHARACTERISTICS OF HISTOGRAM IN FIG. 8

Characteristic	Value
Valid observations:	300
Minimum:	25.616
Maximum:	36.870
Range:	11.253
Median:	29.907
Arithmetic mean:	30.011
Geometric mean:	29.939
Mean square:	4.3885
Variance:	4.4032
Stand. deviation:	2.0984
Coef. of variation:	0.06992
Third moment:	3.3189
Stand. skewness:	0.36101
Fourth moment:	53.755
Stand. kurtosis:	2.7911
Variance of mean:	0.01463
Var. of variance:	8.1236
Var. of 3. moment:	1.5227
Var. of 4. moment:	92.111

The histogram shown in Fig. 9 is evaluated in the same manner as the histogram in Fig. 8, but with the difference that the cut-off limit A2 is applied. A detailed statistical evaluation of the histogram in Fig. 9 is presented in Table VI. The mean

value, standard deviation and coefficient of variation of the histogram in Fig. 9 are plotted on the graphs in Fig. 12, Fig. 13 and Fig. 14.

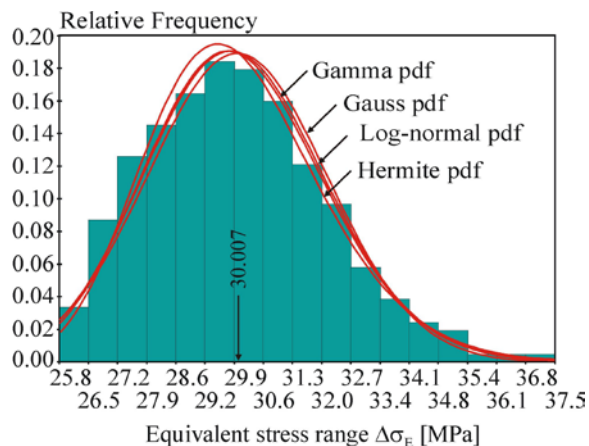


Fig. 9 Histogram for cut-off limit A2, $\nu=0.2$.

It is evident that the histograms in Fig. 8 and Fig. 9 are similar. From a technical point of view, the type of probability density function of the cut-off limit (Gauss or log-normal) has little influence on the statistical evaluation of $\Delta\sigma_E$.

TABLE VI

STATISTICAL CHARACTERISTICS OF HISTOGRAM IN FIG. 9

Characteristic	Value
Valid observations:	300
Minimum:	25.802
Maximum:	37.502
Range:	11.701
Median:	29.893
Arithmetic mean:	30.007
Geometric mean:	29.934
Mean square:	4.4345
Variance:	4.4494
Stand. deviation:	2.1094
Coef. of variation:	0.07029
Third moment:	4.3750
Stand. skewness:	0.46850
Fourth moment:	60.229
Stand. kurtosis:	3.0627
Variance of mean:	0.01478
Var. of variance:	10.377
Var. of 3. moment:	2.3047
Var. of 4. moment:	160.06

The histograms in Fig. 10 and Fig. 11 are processed in a similar manner to the histograms in Fig. 8 and Fig. 9 with the difference that the coefficient of variation $\nu=0.36$ is applied.

A detailed statistical evaluation of the histogram in Fig. 10 is presented in Table VII. A detailed statistical evaluation of the histogram in Fig. 11 is presented in Table VIII.

Fig. 8 to Fig. 11 depict the approximation of histograms using four probability density functions (Hermite, log-normal, Gamma and Gauss) that were not rejected by the goodness of fit tests.

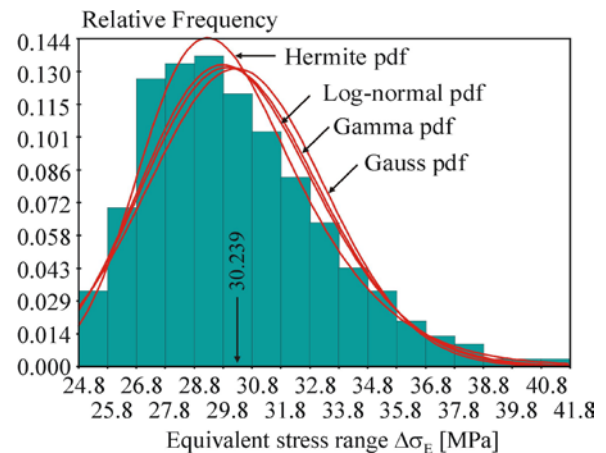


Fig. 10 Histogram for cut-off limit A1, $\nu=0.36$.

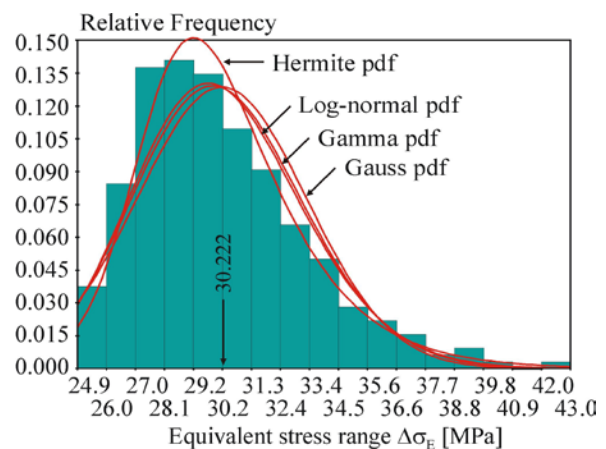


Fig. 11 Histogram for cut-off limit A2, $\nu=0.36$.

TABLE VII

STATISTICAL CHARACTERISTICS OF HISTOGRAM IN FIG. 10

Characteristic	Value
Valid observations:	300
Minimum:	24.779
Maximum:	41.800
Range:	17.022
Median:	29.805
Arithmetic mean:	30.239
Geometric mean:	30.092
Mean square:	9.2559
Variance:	9.2869
Stand. deviation:	3.0474
Coef. of variation:	0.10078
Third moment:	21.266
Stand. skewness:	0.75519
Fourth moment:	297.24
Stand. kurtosis:	3.4695
Variance of mean:	0.03085
Var. of variance:	276.45
Var. of 3. moment:	31.430
Var. of 4. moment:	4838.2

Kolmogorov-Smirnov, Anderson-Darling and Chi-Square goodness of fit tests concluded that neither type of probability density function shown in Fig. 8 to Fig. 11 cannot be rejected reliably. The suitability of probability density function type can also be discussed in connection with the values of skewness and kurtosis of the equivalent stress range, see Fig. 15 and Fig. 16.

The randomness of $\Delta\sigma_E$ is effectively influenced from the value of the coefficient of variation of the cut-off limit ≈ 0.1 . In the limit case, if the cut-off limit has a zero coefficient of variation, the randomness of $\Delta\sigma_E$ is caused only by three random realizations of $\Delta\sigma_E$, where each histogram in Fig. 2 to Fig. 4 leads to one random realization of $\Delta\sigma_E$. Thus, plotting the statistical characteristics of $\Delta\sigma_E$ for small values of the coefficient of variation of the cut-off limit is only indicative in order to present the limit value of the statistical characteristics, see the left part of the graphs in Fig. 12 to Fig. 16. Based on the results in Fig. 15 and Fig. 16, the approximation by the appropriate type of probability density function should not be inferred if the coefficients of variation of the cut-off limit are low.

TABLE VIII

STATISTICAL CHARACTERISTICS OF HISTOGRAM IN FIG. 11

Characteristic	Value
Valid observations:	300
Minimum:	24.914
Maximum:	43.017
Range:	18.103
Median:	29.702
Arithmetic mean:	30.222
Geometric mean:	30.071
Mean square:	9.5875
Variance:	9.6195
Stand. deviation:	3.1015
Coef. of variation:	0.10262
Third moment:	27.472
Stand. skewness:	0.92543
Fourth moment:	366.74
Stand. kurtosis:	3.9898
Variance of mean:	0.03196
Var. of variance:	425.19
Var. of 3. moment:	55.269
Var. of 4. moment:	9966.2

Approximation by Gauss or log-normal probability density functions can be recommended for higher values of the coefficient of variation of the cut-off limit, see Fig. 8 to Fig. 11. Although the log-normal probability density function better approximates the positive values of skewness, it is less suitable for the approximation of the values of kurtosis less than three. Conversely, the Gauss probability density function better reflects the values of kurtosis and worse the values of skewness. However, the differences are not large and other suitable types of bell-shaped probability density functions can be applied if the goodness of fit tests do not reject such a choice. Furthermore, the question of the appropriate type of probability density function can be discussed again in the

future and addressed by goodness of fit tests using current measurement data.

Coefficient of variation 0.05 to 0.1 of the equivalent stress range $\Delta\sigma_E$ can be considered in the case study presented here. If more specific information is unavailable, the coefficient of variation of the equivalent stress range $\Delta\sigma_E$ can be considered as approximately 0.1 in stochastic models, see for e.g. [31, 32]. This coefficient of variation corresponds approximately to the coefficient of variation of the cut-off limit of about 0.2 with a slight increase due to additional uncertainties arising from the uncertainties of the conditions of the long-term monitoring program, which result in a higher value of the coefficient of variation.

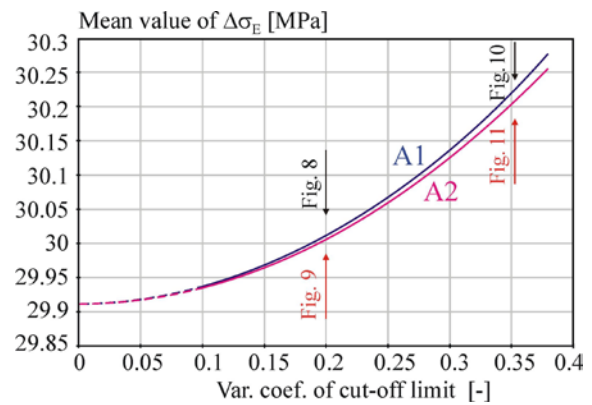


Fig. 12 Var. coeff. of cut-off limit vs mean value of $\Delta\sigma_E$

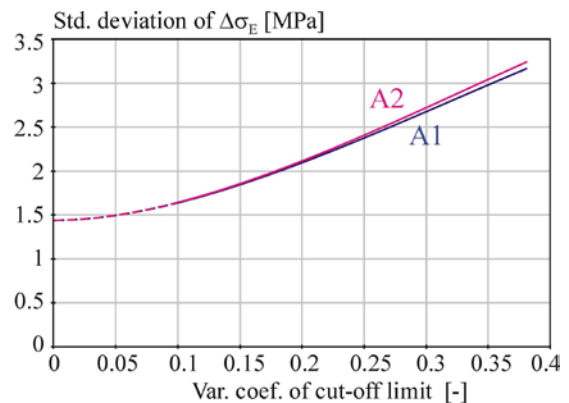


Fig. 13 Var. coeff. of cut-off limit vs std. deviation of $\Delta\sigma_E$

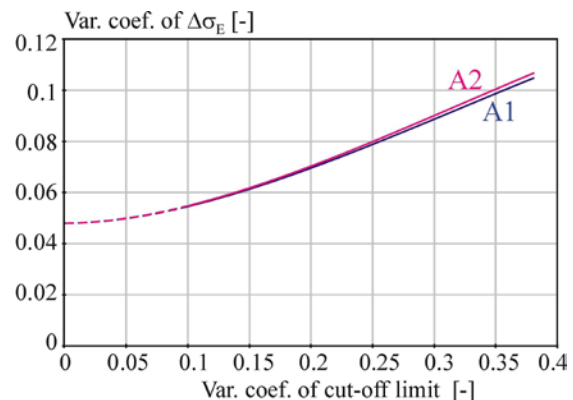


Fig. 14 Var. coeff. of cut-off limit vs var. coeff. of $\Delta\sigma_E$

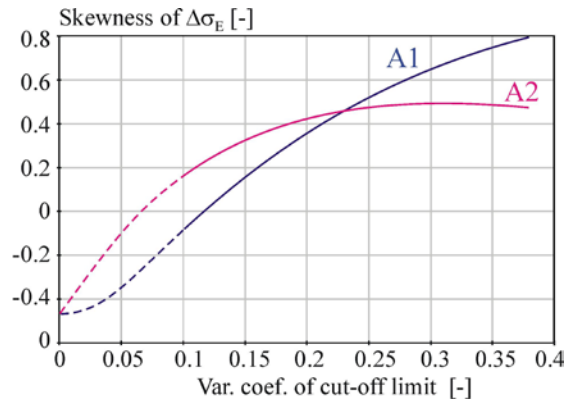


Fig. 15 Var. coeff. of cut-off limit vs skewness of $\Delta\sigma_E$

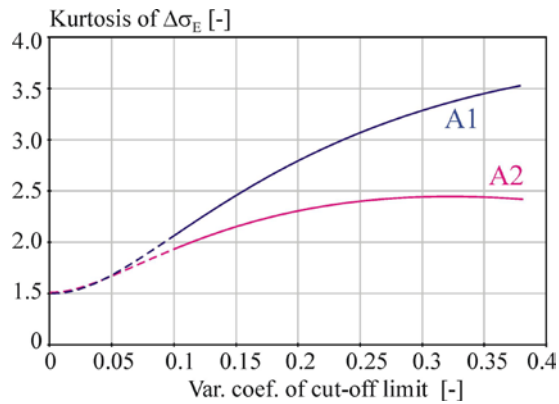


Fig. 16 Var. coeff. of cut-off limit vs kurtosis of $\Delta\sigma_E$

IV. CONCLUSION

The presented case study showed that the uncertainty of the equivalent stress range $\Delta\sigma_E$ can be modelled with a coefficient of variation from 0.05 to 0.1.

It is shown in the paper that the obtained value of the coefficient of variation [0.05, 0.1] is given by uncertainties present in the statistical evaluation of the histogram of the stress range spectrum. The coefficient of variation may be increased in connection with other uncertainties of the long-term monitoring program performed during the operational period of the bridge. It is very intuitive that increasing the coefficient of variation may be significant when the monitoring program is burdened with greater uncertainty, for example, with regard to changes in the expected traffic load. The traffic load can vary (grow) during the lifetime of the bridge, but may be limited at the end of the lifetime for safety reasons if the bridge exhibits large fatigue failure whose repair is no longer economical.

Gauss or log-normal probability density function with coefficient of variation 0.1 of equivalent stress range $\Delta\sigma_E$ can be recommended for practical use in most theoretical stochastic computational models if more accurate information on uncertainties of data from the monitoring program is unavailable.

The case study showed a methodology for the statistical analysis of the random variability of the equivalent stress range $\Delta\sigma_E$, which can be further discussed and developed. Based on

the presented methodology, the random variability of the equivalent stress range $\Delta\sigma_E$ can also be analysed in other case studies using input data from measurements.

ACKNOWLEDGMENT

This result was achieved with the financial support of the projects GAČR 17-01589S and No. LO1408 “AdMAs UP”.

REFERENCES

- [1] W.E. Nyman, F. Moses, “Calibration of bridge fatigue design model,” *Journal of Structural Engineering*, vol. 11, pp. 1251–1266, 1985.
- [2] S.K. Raju, F. Moses, C.G. Schilling, “Reliability calibration of fatigue evaluation and design procedures,” *Journal of Structural Engineering*, vol. 116, pp. 1356–1369, 1990.
- [3] T.D. Righiniotis, “Effects of increasing traffic loads on the fatigue reliability of a typical welded bridge detail,” *International Journal of Fatigue*, vol. 28, no. 8, pp. 873–880, 2006.
- [4] V. G. Rao, S. Talukdar, “Prediction of fatigue life of a continuous bridge girder based on vehicle induced stress history,” *Shock and Vibration*, vol. 10, pp. 325–338, 2003.
- [5] J. Leander, M. Al-Emrani, “Reliability-based fatigue assessment of steel bridges using LEFM – A sensitivity analysis,” *International Journal of Fatigue*, vol. 93, pp. 82–91, 2016.
- [6] J. Leander, “Reliability evaluation of the Eurocode model for fatigue assessment of steel bridges,” *Journal of Constructional Steel Research* vol. 141, pp. 1–8, 2018.
- [7] J.H. Kim, M.C. Jeong, T.H. Lee, W.W. Lee, J.S. Kong, “Development of fatigue prediction model for steel bridges based on characteristics of variable stress spectra,” *International Journal of Damage Mechanics*, vol. 26, no. 7, pp. 951–967, 2017.
- [8] W. Nagy, B. Wang, B. Culek, P. Van Bogaert, H. De Backer, “Development of a fatigue experiment for the stiffener-to-deck plate connection in orthotropic steel decks,” *International Journal of Steel Structures*, vol. 17, no. 4, pp. 1353–1364, 2017.
- [9] H. Hasni, A. H. Alavi, P. Jiao, N. Lajnef, “Detection of fatigue cracking in steel bridge girders: A support vector machine approach,” *Archives of Civil and Mechanical Engineering*, vol. 17, no. 3, pp. 609–622, 2017.
- [10] D. Hajializadeh, E.J. O'Brien, A.J. O'Connor, “Virtual structural health monitoring and remaining life prediction of steel bridges,” *Canadian Journal of Civil Engineering*, vol. 44, no. 4, pp. 264–273, 2017.
- [11] M. Bitarafan, S.H. Zolfani, S.L. Arefi, E.K. Zavadskas, A. Mahmouzdadeh, “Evaluation of real-time intelligent sensors for structural health monitoring of bridges based on SWARA-WASPAS; a case in Iran,” *Baltic Journal of Road and Bridge Engineering*, vol. 99, no. 4, pp. 333–340, 2014.
- [12] J. Antucheviciene, Z. Kala, M. Marzouk, E.R. Vaidogas, “Solving civil engineering problems by means of fuzzy and stochastic MCDM methods: Current state and future research,” *Mathematical Problems in Engineering*, vol. 2015, Article ID 362579, p. 16, 2015.
- [13] J. Antucheviciene, Z. Kala, M. Marzouk, E.R. Vaidogas, “Decision making methods and applications in civil engineering,” *Mathematical Problems in Engineering*, vol. 2015, Article ID 160569, p. 3, 2015.
- [14] E.K. Zavadskas, J. Antucheviciene, T. Vilutiene, H. Adeli, “Sustainable decision-making in civil engineering, construction and building technology,” *Sustainability*, vol. 10, no. 1, p. 21, 2016.
- [15] S. Seitl, P. Miarka, L. Malková, M. Krejsa, “Comparison of calibration functions for short edge cracks under selected loads,” *Key Engineering Materials*, vol. 754, pp. 353–356, 2017.
- [16] S. Seitl, P. Miarka, Z. Kala, J. Klusák, “Effect of rivet holes on calibration curves for edge cracks under various loading types in steel bridge structure,” *Procedia Structural Integrity*, vol. 5, pp. 697–704, 2017.
- [17] S. Seitl, P. Miarka, Z. Kala, “Geometry functions for edge cracks in steel bridge under three- and four- point bending with various span,” *Transactions of the VSB – Technical University of Ostrava, Civil Engineering Series*, vol. 18, no. 2, pp. 44–49, 2018.
- [18] K. Kwon, D. M. Frangopol, “Bridge fatigue reliability assessment using probability density functions of equivalent stress range based on field

- monitoring data,” *International Journal of Fatigue*, vol. 32, pp. 1221–1232, 2010.
- [19] J. Leander, “A decision support framework for fatigue assessment of steel bridges,” *Engineering Failure Analysis*, vol. 91, pp. 306–314, 2018.
- [20] P. C. Paris and F. Erdogan, “A critical analysis of crack propagation laws,” *Journal of Basic Engineering*, vol. 85, no. 4, pp. 528–534, 1963.
- [21] D. Kocanda, V. Hutsaylyuk, T. Slezak, J. Torzewski, H. Nykyforchyn, V., Kyryliv, “Fatigue crack growth rates of S235 and S355 steels after friction stir processing”, *Materials Sciences Forum*, vol. 726, pp. 203–210, 2012.
- [22] D. Broek, *Elementary Engineering Fracture Mechanics*, Martinus Nijhoff, Dordrecht, The Netherlands, 4th edition, 1986.
- [23] H. Tada, P.C. Paris, G.R. Irwin, *The stress analysis of cracks handbook*, New York: ASME Press, 2000.
- [24] Y. Murakami, *Stress intensity factors handbook*, New York: Pergamon Press, 1986.
- [25] 25EN 1993-1:2005. Eurocode 3: Design of steel structures – Part 1-9: Fatigue.
- [26] A. Wöhler, “Versuche über die Festigkeit von Eisenbahnwagen-Achsen,” *Zeitschrift Bauwesen*, vol. 10, 1860.
- [27] M. Soliman, D. Frangopol, K. Kown, “Fatigue assessment and service life prediction of existing steel bridges by integrating SHM into a probabilistic bilinear S-N approach,” *Journal of Structural Engineering*, vol. 139, no. 10, pp. 1728–1740, 2013.
- [28] T.D. Righiniotis, M.K. Chryssanthopoulos, “Probabilistic fatigue analysis under constant amplitude loading,” *Journal of Constructional Steel Research*, vol. 59, no. 7, pp. 867–886, 2003.
- [29] M.D. McKey, W.J. Conover, R.J. Beckman “A comparison of the three methods of selecting values of input variables in the analysis of output from a computer code,” *Technometrics*, vol. 21, pp. 239–245, 1979.
- [30] R.C. Iman, W.J. Conover, “Small sample sensitivity analysis techniques for computer models with an application to risk assessment,” *Communications in Statistics – Theory and Methods*, vol. 9, no. 17, pp. 1749–1842, 1980.
- [31] M. Krejsa, L. Koubova, J. Flodr, J. Protivinsky, Q.T. Nguyen, “Probabilistic prediction of fatigue damage based on linear fracture mechanics,” *Frattura ed Integrita Strutturale*, vol. 11, no. 39, pp. 143–159, 2017.
- [32] Z. Kala, “Global sensitivity analysis of reliability of structural bridge system,” *Engineering Structures*, vol. 194, pp. 36–45, 2019.